Fisheye lens calibration using virtual grid

Aymen Arfaoui[1,2] and Simon Thibault[2,3,*]

[1]Department of Geomatics, Laval University, Québec, QC G1V0A6, Canada

[2]Center for Optics, Photonics and Lasers, Laval University, Québec, QC G1V0A6, Canada

[3]Department of Physics, Engineering Physics and Optics, Laval University, Québec, QC G1V0A6, Canada

*Corresponding author: Simon.Thibault@phy.ulaval.ca

Received 29 January 2013; revised 27 February 2013; accepted 5 March 2013;
posted 5 March 2013 (Doc. ID 184279); published 12 April 2013

We present herein a technique to calibrate fisheye lenses using cross diffractive optical elements. The setup generated a robust and accurate virtual calibration grid, and the calibration was performed by rotating the camera around two axes. We propose a comparison of three fisheye mathematical models and an evaluation of the number of images in the calibration process. The comparison of our experimental data according to the 3D calibration object results showed that our technique is efficient and reliable. © 2013 Optical Society of America

OCIS codes: (050.0050) Diffraction and gratings; (040.1490) Cameras; (150.1488) Calibration.
http://dx.doi.org/10.1364/AO.52.002577

1. Introduction

A fisheye lens is a refractive optical system that provides a wide field-of-view (FOV) of about 180 deg and has a very large apparent depth of field, which gives clear pictures without focus adjustment. Therefore, it is used in mobile robots, intelligent vehicles, surveillance, and so on. In many such applications that involve accurate quantitative measurements, fisheye camera calibration is a crucial step.

The required accuracy and the nature of the application are the main determinants of the model and the method of fisheye calibration. When lens distortion is not considered, camera calibration consists of estimation of the perspective projection that represents the relationship between the target coordinates space and their projection in the image [1]. This projection is based on the fact that the angle of incidence of the ray from an object point is equal to the angle between the ray and the optical axis. However, the radial distortion component for the fisheye lens is relatively high. Therefore, other projection models were developed and can be divided into three types. The first type is called the radial fisheye model, and it describes conversion from the perspective radial distance of a point in the image to its fisheye distorted image, using methods such as the polynomial fisheye transform [2] or the division model [3]. The second type is the fisheye projection, and it is based on the principle that the radial distance of an image point depends on the angle of incidence of the ray. The equidistant [4], equisolid [5], orthographic [6], and stereographic [7] models could be briefly mentioned as examples of this. The third type is the FOV model [8] when the radial distance depends on the FOV of the camera. However, this model is not sufficient to model the complex distortion of the fisheye lens. To this end, we recommend using a combination of polynomial and FOV models [9].

Previous work has shown that fisheye calibration can be performed by using one or several images of a known or an unknown pattern. A calibration room that includes known 3D control points can be established and used to calibrate a fisheye camera with only one image [10]. When a known 2D calibration object is used, the camera is fixed and different images can be captured. For each image, the object is placed at different positions and orientations to produce a set of noncoplanar points needed for

1559-128X/13/122577-07$15.00/0
© 2013 Optical Society of America

the nonlinear minimization algorithms [11]. If the target coordinates in the pattern are unknown, the estimation of camera parameters is called auto-calibration. A set of reliable point pairs in a sequence of images is sufficient to find intrinsic parameters [12–14]. Other kinds of methods used the property that the images of parallel lines converge at two vanishing points, and the line that intersects the two vanishing points also intersects the optical center [15]. Calibration is herein performed by observing two sets of lines in horizontal and vertical directions [16].

In order to get a stable, accurate, and compact calibration object, a new setup using cross diffractive optical elements (CDOEs) has recently been proposed and implemented in our laboratory [17]. This idea of calibrating a camera from DOEs was introduced in 2008 by Bauer *et al.* [18]. This laser-based technique requires only a very limited space, which is very efficient to calibrate when an object at infinity is involved. This is particularly true with long focal length lenses where a very large room is required for calibration. The CDOE also has another advantage over targets on a screen. Target positions must be measured with high precision prior to calibration. Each target will have a residual error associated with the measurement method. In the case of CDOE, the position of each diffractive order is determined by the characteristic of the diffraction gratings. The error on the position of each diffractive order is perfectly determined and only determined by the grating equation. Consequently, the CDOE method will not suffer from random errors due to measurement errors of the calibration targets.

In the case of a fisheye, the short focal length produces a small hyperfocal distance and the calibration will not require an object at infinity. The hyperfocal distance is a convenient approximation of infinity based on the depth-of-focus definition. Except in the telecentric fisheye, the calibration can be affected over the depth of focus. Consequently, for very high precision, the calibration must be done using a target at infinity. The CDOE method overcomes this difficulty by imposing real targets located at infinity, which gives precise calibration control points. The calibration problem is then reduced accurately to one of nontranslating camera calibration. The CDOE allows different viewing directions simultaneously and provides a very accurate diffraction pattern.

This study aims at exploiting these aforementioned advantages to calibrate fisheye cameras. We propose a technique that requires the diffractive optical virtual grid to be observed by the camera at a few different orientations to cover the wide FOV of the camera. In our previous work [17], we used the CDOE to calibrate a wide-angle lens that had a 60 deg full FOV using a single image. This work will use a different approach to calibrate a panoramic lens with a 180 deg FOV. We define in Section 2 the procedure to cover the entire FOV of the fisheye camera using a diffraction pattern. Section 3 presents the mathematical model. Once the mathematical model of the camera calibration using CDOEs was optimized, the calibration procedure was performed in Section 4. Section 5 shows the experimental results and discussion of the calibration approach.

2. Setup for Fisheye Calibration

The calibration pattern consisted of 15 × 15 equally spaced dots. The camera was mounted in an object to allow rotation around two axes as shown in Fig. 1. Detailed setup description can be found in [17].

Since the fisheye lens has a hemispherical view and in order to achieve an accurate calibration, more than one image is needed to fulfill the whole FOV. For each camera rotation angle, one image was taken. Figure 2 illustrates the 15 × 15 grid position in the image for nine rotation angles (R0 to R8).

3. Fisheye Calibration with CDOE

A. Calibration Pattern

Following the use of two crossed gratings, Thibault *et al.* [17] have shown that the diffractive orders produced by the first grating were not exactly perpendicular to the orders produced by the second grating.

Every spot is a point at infinity and can be presented in homogeneous coordinates:

$$P = [X, Y, Z, 0]^T, \tag{1}$$

where

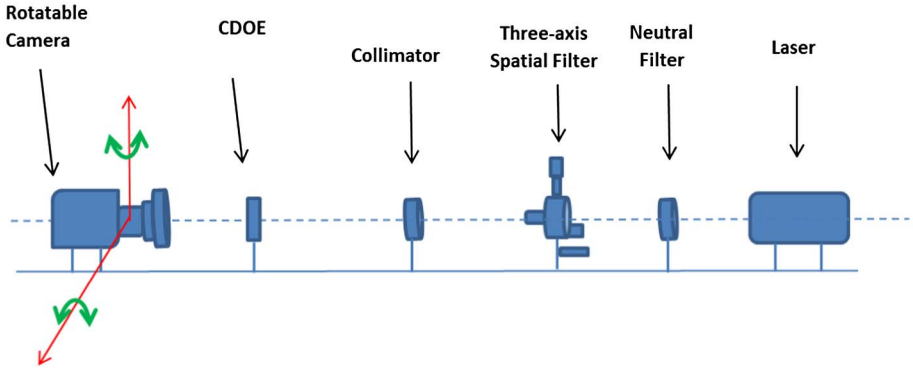

Fig. 1. Calibration setup with rotatable camera.

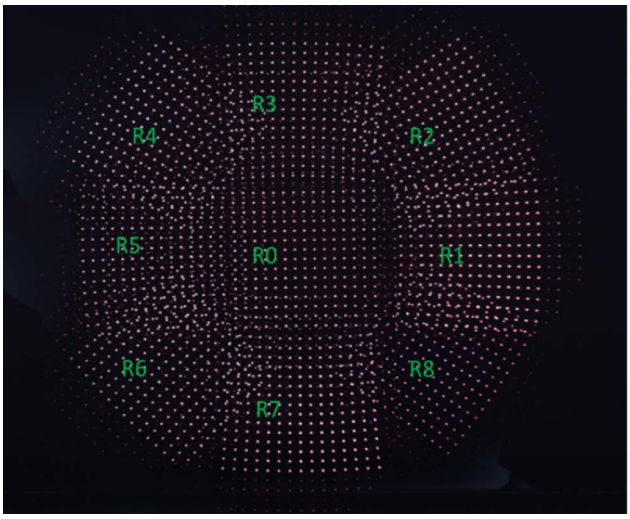

Fig. 2. Layout of the grid images recorded by fisheye camera in nine different orientations.

$$X = \lambda f_x + r_x + (\lambda f_y + r_y)\sin(\alpha), \tag{2}$$

$$Y = (\lambda f_y + r_y)\cos(\alpha), \tag{3}$$

$$Z = (1 - (X^2 + Y^2))^{1/2}, \tag{4}$$

where f_x and f_y are the grating's spatial frequencies, λ is the wavelength of the laser beam, r_x and r_y are errors caused by the nonperpendicular incidence of the laser beam to the DOE plane in x and y directions with respect to the optical axis (z), and α is the clocking error between the two gratings (in rotation around the z axis).

B. Fisheye Projection

Fisheye lenses do not obey the pinhole geometry; they instead, and usually, follow an equidistant projection as

$$r = f\theta, \tag{5}$$

where θ is the angle between the incident ray and the optical axis, r is the radial or polar distance between the image point and the principal point, and f is the focal length.

Occasionally, other projections were used where the sine or the tangent of the incident angle is related to the radial distance in the image by a constant (equisolid, orthographic, and stereographic models). Therefore we consider projections in the general form as follows:

$$r = k_1\theta + k_2\theta^3 + k_3\theta^5 + \cdots, \tag{6}$$

where k_1 is very close to the focal length. $k_2, k_3, \ldots$ are the distortion coefficients. The order of the polynomial can be determined experimentally.

C. Projection Procedures

The fisheye calibration is the determination of the mapping model between points in a world coordinate system and their corresponding elements in an image coordinate system. It is characterized by four transformations (Fig. 3):

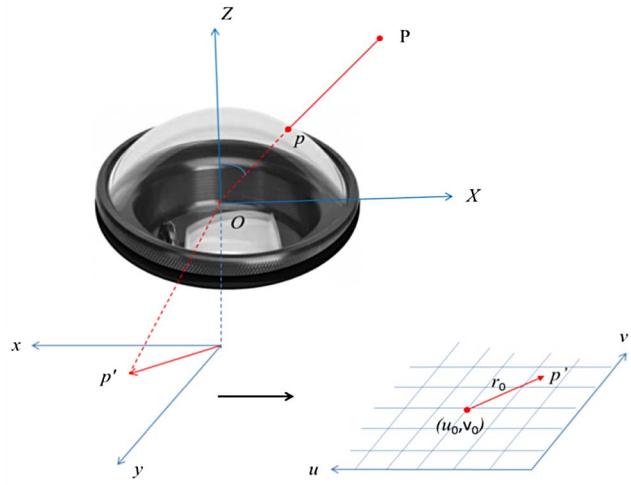

Fig. 3. Fisheye projection.

- The beam directions P are transformed into a camera coordinate system with the relative rotation R:

$$P' = \begin{pmatrix} R_{3\times3} & 0 \\ 0 & 1 \end{pmatrix} \cdot P. \tag{7}$$

- P' is projected to a point p on a unit sphere centered at the viewpoint O:

$$p = [\sin\theta\cos\varphi, \sin\theta\sin\varphi, \cos\theta]^T. \tag{8}$$

- By assuming that the pixel coordinate system is orthogonal, the relation between image coordinates $[x, y]$ in millimeters and image coordinates $[u, v]$ in pixels is given by an affine transformation as

$$\begin{pmatrix} u \\ v \end{pmatrix} = \begin{pmatrix} \alpha_u & 0 \\ 0 & \alpha_v \end{pmatrix}\begin{pmatrix} x \\ y \end{pmatrix} + \begin{pmatrix} u_0 \\ v_0 \end{pmatrix}, \tag{9}$$

where $[u_0, v_0]^T$ are the pixel coordinates of the principal point, and (α_u, α_v) are the scale factors of the image axes u and v in pixels.

The goal of fisheye camera calibration is to compute intrinsic and extrinsic parameters. The intrinsic parameters describe the internal camera's geometric and optical characteristics (focal length, scales factor and principal point, distortion coefficients). The extrinsic parameters include the position and orientation of the camera (rotation matrix).

4. Calibration Algorithm

As mentioned before, the fisheye calibration is the estimation of the extrinsic parameters that describe the orientation of the camera frame relative to the CDOE coordinate system (matrix R), as well as the intrinsic parameters $(u_0, v_0, k_1, k_2, k_3 \ldots)$. The process is solved by taking N images of the CDOE pattern in

different orientations. In each image, M control points (15×15 spots) were observed. We used the centroid algorithm to achieve image data extraction [11]. The unknown parameters were estimated iteratively with the nonlinear least-squares adjustment method. We have optimized the following function:

$$E_{\text{tot}} = \sum_{k=1}^{N} \sum_{j=1}^{M} (r_{cjk} - r_{ojk})^2, \tag{10}$$

where $r_c = [(u - u_0)^2 + (v - v_0)^2]^{1/2}$ is the radial distance computed by the model, and r_o is the radial distance observed or measured in the image.

The accuracy evaluation was based on the root-mean-square error (RMSE) calculated from the residuals. Each residual is the difference between observed and computed pixel coordinates. The following diagram (Fig. 4) illustrates the steps for fisheye camera calibration.

5. Results and Discussion

The calibration algorithm was applied to a fisheye lens with an effective focal length of 1.87 mm ($f/2.8$) and a 180 deg angle of view. The dimension of its image is 1944×2592 pixels. The pixel size is 0.0022 mm.

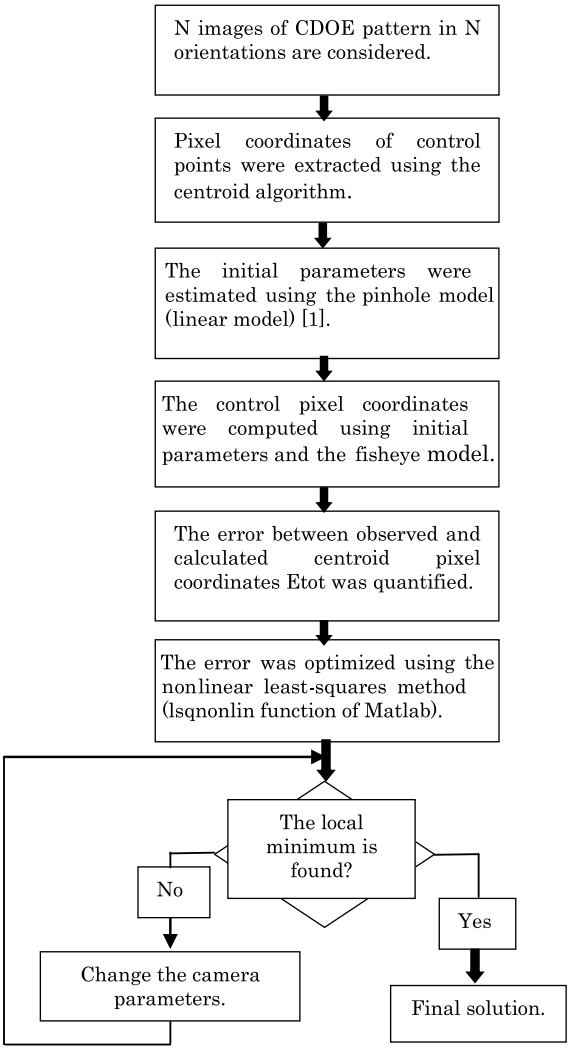

Fig. 4. Diagram of calibration algorithm.

Since the distribution of control points has a strong effect on the calibration accuracy, nine images were taken in varying orientations to fulfill the entire FOV of the fisheye camera (Fig. 2).

A set of 15×15 points per image gave $225 \times N$ pairs (r_c, r_o) [Eq. (10)]. The image coordinates were calculated with subpixel accuracy using a centroid algorithm in gray-scale mode. Figure 5 shows the computed pixel coordinates for all of the nine images taken.

The effect of the number of images on the calibration process was studied by comparing four cases:

- Case 1: calibration using four images (R2, R4, R6, and R8)
- Case 2: five images (R0, R2, R4, R6, and R8)
- Case 3: eight images (R1, R2, R3, R4, R5, R6, R7, and R8)
- Case 4: nine images (R0, R1, R2, R3, R4, R5, R6, R7, and R8)

The accuracy of the general model and the impact of the polynomial degree on the RMSE were examined using the following:

- First-order polynomial (equidistant model): $r = k_1\theta$
- Third-order polynomial: $r = k_1\theta + k_2\theta^3$
- Fifth-order polynomial: $r = k_1\theta + k_2\theta^3 + k_3\theta^5$.

The intrinsic parameters and the corresponding RMSE have been computed for the four image combinations and for the different models. Tables 1–3 illustrate the results in pixels.

Interestingly and as shown in Tables 1–3, the results using eight and nine images were very close. It can be noted also that the fifth-order model returns the lowest error (Table 3), as expected. However, the accuracy improvement of this model is not very high compared to the third-order and the equidistant models. The residuals for each control point using eight images and the equidistant model are shown

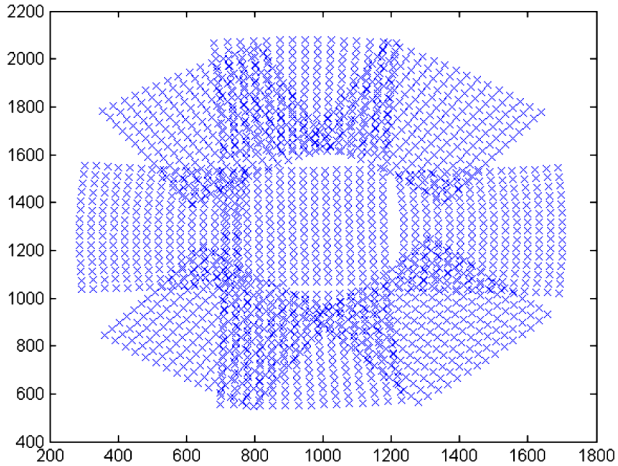

Fig. 5. Pixel coordinates for all images computed by centroid algorithm.

Table 1. Calibration Results Using the Equidistant Model

	Four Images	Five Images	Eight Images	Nine Images
u_o	1336.04	1340.40	1340.06	1340.47
v_o	925.85	924.61	924.54	924.38
k_1	847.83	858.76	843.67	843.67
RMSE	0.180	0.181	0.183	0.187

Table 2. Calibration Results Using the Third-Order Model

	Four Images	Five Images	Eight Images	Nine Images
u_o	1336.68	1338.80	1339.90	1340.32
v_o	925.33	924.10	923.95	924.22
k_1	857.68	865.17	862.79	862.63
k_2	−10.14	−10.26	−12.42	−14.44
RMSE	0.128	0.149	0.155	0.162

Table 3. Calibration Results Using the Fifth-Order Model

	Four Images	Five Images	Eight Images	Nine Images
u_o	1338.29	1339.69	1340.04	1340.11
v_o	923.94	923.95	924.58	924.22
k_1	858.98	864.23	862.74	862.37
k_2	−10.84	−11.20	−13.69	−13.67
k_3	−0.40	−0.41	0.79	0.78
RMSE	0.137	0.138	0.147	0.149

in Fig. 6. The figure shows the residual in pixels (Y axis) for all 225 points (X axis) and for different camera orientations (R0 to R8).

Tables 1,2, and 3 illustrate the results obtained as a function of the number of images used in the computation. Many other combinations of images are studied, and the results show that the stability is ensured with a large number of well-distributed control points (cases 3 and 4, for example).

The results from the virtual grid results were compared to a 3D calibration object (the focus of the lens is the same for both measurements). This calibration object consisted of 339 targets regularly spaced on perpendicular walls as shown in Fig. 7. Their geometry in 3D space is known with very good precision (between 0.04 and 0.08 mm). For determination of the target centers giving the control-point values, the ellipse method was used [19]. We applied the calibration algorithm (Fig. 4) to this set of targets.

The results of both methods were compared. Table 4 shows the calibration parameters. Using the same algorithm but with different calibration objects, we observed that the CDOE method always returns the lowest residual errors, as shown in Table 5. It seems that we have a different RMSE of 0.08 pixels between the two methods. This error is quite small, but we have it in all cases. The difference is not significant and cannot be used to clearly state that the CDOE method is better. However, it clearly shows that the CDOE can be used with success to calibrate a fisheye camera with results that are as good as those of a standard 3D object method.

The RMSE of our technique is comparable to the results reported by Schneider *et al.* [4] and Kannala and Brandt [14].

Moreover, to calibrate a camera like a fisheye with only one image, we must use a calibration setup with appropriate dimensions and shape, which is sometimes less convenient. However, most studies have used several observations with different orientations to estimate the camera parameters, and they showed that the results are more accurate. The CDOE produces 225 points per frame and allows different

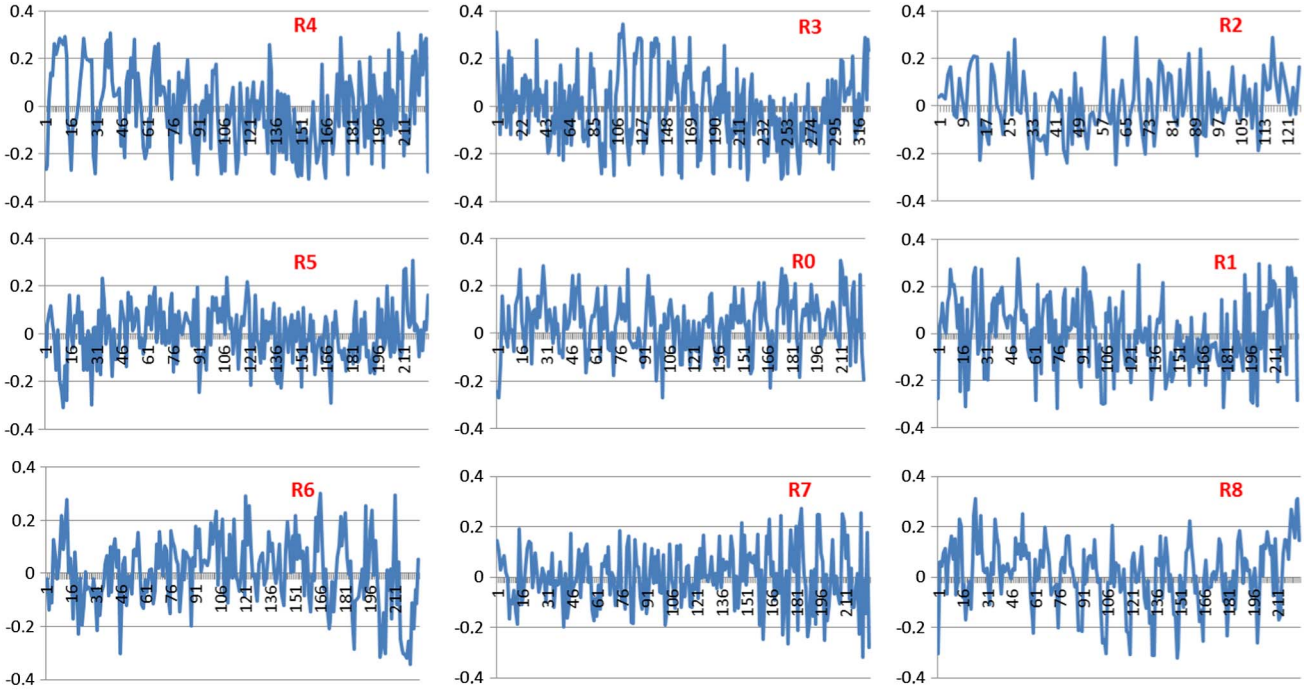

Fig. 6. Remaining residuals for all images after calibration (in pixels).

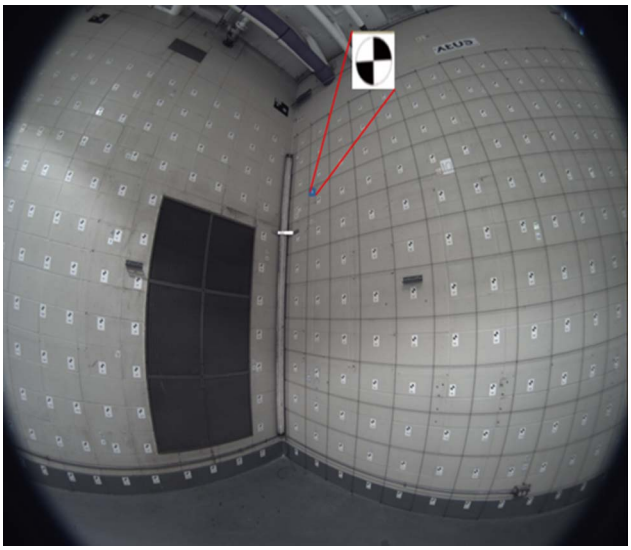

Fig. 7. Targets of the 3D calibration object.

Table 4. Calibration Comparison

	u_o	v_o	k_1	k_2	k_3
CDOE	1340.04	924.58	862.74	−13.69	0.79
3D object	1339.89	924.01	862.33	−12.95	0.48

Table 5. RMSE for Fisheye Camera Calibration Using CDOE and 3D Object

	First-Order Model	Third-Order Model	Fifth-Order Model
RMSE using CDOE	0.183	0.155	0.147
RMSE 3D using object	0.263	0.242	0.239

viewing directions simultaneously. We have shown that only eight images, with this large number of control points (225×8), produced a completely and accurately calibrated fisheye camera.

The calibration accuracy depends on the way the control points are measured. Several location methods have been proposed. They were sometimes complex and have provided subpixel accuracy. The DOE herein produces light spots on a black background. The control-point coordinates are easily estimated with subpixel accuracy using a centroid algorithm in gray-scale mode. The accuracy can be improved in the future using other techniques of pixel coordinate measurements such as adaptive thresholding and dynamic windowing methods [20].

6. Conclusions

In this study, we have described a method using a compact calibration object for fisheye lens calibration. The proposed setup is based on two commercially available diffractive optical elements in a crossed configuration that generates a robust and accurate virtual grid suitable for camera calibration. The calibration procedure was successfully applied to real images acquired by rotating the camera. A comparison of three models and an evaluation of the effect of the number of images on the calibration process were performed using this technique. The experimental results and the comparison with a 3D calibration object showed that the virtual grid method is efficient and reliable.

The principal limiting factor of this technique is that only one image is not enough to calibrate a fisheye camera. The required accuracy and the nature of the application are used to choose the number of images required for the calibration procedure. Consequently, this technique can be adopted to calibrate different lens types with any FOV (wide-angle and omnidirectional cameras) using images taken by rotating the camera.

The size of the CDOE can also limit the size of the fisheye that can be calibrated using our technique. As discussed in the previous paper [17], the technique will work as long as the entrance pupil of the fisheye can be illuminated by the CDOE (see Fig. 1 and Eq. (1) of [17]). Even for a large format fisheye, the entrance pupil is small compared to the front lens diameter. Moreover, the entrance pupil position (from the first lens surface) is also close to the front surface. With our CDOE, we can illuminate a 12 mm entrance pupil as far as 65 mm of the front optical surface of the fisheye. This corresponds to a fisheye ($f/2.8$) of 34 mm focal length. Consequently, our technique can also be used to calibrate a larger format fisheye.

In future work, the virtual object grids of dots produced by the CDOE will be used to calibrate zoom cameras. We also intend to test the reliability of this technique for stereo system calibration.

References

1. R. Jain, R. Kasturi, and B. G. Schunck, *Machine Vision* (McGraw-Hill, 1995).
2. A. Basu and S. Licardie, "Modeling fish-eye lenses," in *International Conference on Intelligent Robots and Systems '93*, Yokohama, Japan, 26–30 July (IEEE, 1993), pp. 1822–1828.
3. A. W. Fitzgibbon, "Simultaneous linear estimation of multiple view geometry and lens distortion," in *Proceedings of the 2001 IEEE Computer Society Conference on Computer Vision and Pattern Recognition* (IEEE, 2001), pp. 125–132.
4. D. Schneider, E. Schwalbe, and H. G. Maas, "Validation of geometric models for fisheye lenses," ISPRS J. Photogramm. Remote Sens. **64**, 259–266 (2009).
5. C. Hughes, P. Denny, M. Glavin, and E. Jones, "Equidistant fish-eye calibration and rectification by vanishing point extraction," IEEE Trans. Pattern Anal. Mach. Intell. **32**, 2289–2296 (2010).
6. S. K. Nayar, "Catadioptric omnidirectional camera," in *Proceedings of IEEE Computer Society Conference on Computer Vision and Pattern Recognition* (IEEE, 1997), pp. 482–488.
7. M. M. Fleck, "Perspective projection: the wrong imaging model," Technical report 95-01 (University of Iowa, 1995).
8. A. Basuand and S. Licardie, "Alternative models for fish-eye lenses," Pattern Recogn. Lett. **16**, 433–441 (1995).
9. F. Devernay and O. Faugeras, "Straight lines have to be straight," Mach. Vis. Appl. **13**, 14–24 (2001).
10. E. Schwalbe, "Geometric modelling and calibration of fisheye lens camera systems," in Proceedings of 2nd Panoramic Photo-

grammetry Workshop, International Archives of Photogrammetry, Remote Sensing and Spatial Information Sciences 36, Part 5/W8 (2005).
11. J. Kannala and S. S. Brandt, "A generic camera calibration method for fish-eye lenses," in *International Conference on Pattern Recognition, 2004* (Cambridge, 2004), pp. 10–13.
12. B. Micusik and T. Pajdla, "Structure from motion with wide circular field of view cameras," IEEE Trans. Pattern Anal. Mach. Intell. **28**, 1135–1149 (2006).
13. H. Li and R. Hartley, "Plane-based calibration and auto-calibration of a fish-eye camera," in *7th Asian Conference on Computer Vision* (Springer, 2006), Vol. **3851**, pp. 21–30.
14. J. Kannala and S. S. Brandt, "A generic camera model and calibration method for conventional, wide-angle, and fish-eye lenses," IEEE Trans. Pattern Anal. Mach. Intell. **28**, 1335–1340 (2006).
15. C. Hughes, P. Denny, E. Jones, and M. Glavin, "Accuracy of fish-eye lens models," Appl. Opt. **49**, 3338–3347 (2010).
16. J. Yang and Z. Liu, "Fisheye camera calibration with two pairs of vanishing points," in *International Conference on Information Technology and Computer Science 2009* (IEEE, 2009), Vol. **1**, pp. 321–324.
17. S. Thibault, A. Arfaoui, and P. Désaulniers, "Cross-diffractive optical elements for wide angle geometric camera calibration," Opt. Lett. **36**, 4770–4772 (2011).
18. M. Bauer, D. Grießbach, A. Hermerschmidt, S. Krüger, M. Scheele, and A. Schischmanow, "Geometrical camera calibration with diffractive optical elements," Opt. Express **16**, 20241–20248 (2008).
19. A. Arfaoui and F. Plante, "Camera calibration using composed cubic splines," Geomatica **65**, 189–197 (2011).
20. A. Vyas, M. B. Roopashree, and B. R. Prasad, "Centroid detection by Gaussian pattern matching in adaptive optics," Int. J. Comput. Appl. **1**, 30–35 (2010).